Catalysis Science & Technology

ROYAL SOCIETY OF CHEMISTRY

PAPER

View Article Online
View Journal | View Issue

Cite this: *Catal. Sci. Technol.*, 2020, 10, 6533

D-Phenylglycine aminotransferase (D-PhgAT) – substrate scope and structural insights of a stereo-inverting biocatalyst used in the preparation of aromatic amino acids†‡

Annabel Serpico,§[a] Silvia De Cesare,[a] Jon Marles-Wright,[b] M. Kalim Akhtar,¶[c] Gary J. Loake[c] and Dominic J. Campopiano *[a]

Received 10th July 2020,
Accepted 27th July 2020

DOI: 10.1039/d0cy01391a

rsc.li/catalysis

Enantiopure amines are key building blocks in the synthesis of many pharmaceuticals, so a route to their production is a current goal for biocatalysis. The stereo-inverting D-phenylglycine aminotransferase (D-PhgAT), isolated from *Pseudomonas stutzeri* ST-201, catalyses the reversible transamination from L-glutamic acid to benzoylformate, yielding α-ketoglutarate and D-phenylglycine (D-Phg). Detailed kinetic analysis revealed a range of amine donor and acceptor substrates that allowed the synthesis of enantiopure aromatic D-amino acids at a preparative scale. We also determined the first X-ray crystal structure of D-PhgAT with its bound pyridoxal 5′-phosphate (PLP) cofactor at 2.25 Å resolution. A combination of structural analysis and site-directed mutagenesis of this class III aminotransferase revealed key residues that are potentially involved in the dual substrate recognition, as well as controlling the stereo-inverting behaviour of D-PhgAT. Two arginine residues (Arg34 and Arg407) are involved in substrate recognition within P and O binding pockets respectively. These studies lay the foundation for further enzyme engineering and promote D-PhgAT as a useful biocatalyst for the sustainable production of high value, aromatic D-amino acids.

Introduction

The non-proteinogenic amino acids D-phenylglycine (D-Phg) and D-4-hydroxyphenylglycine (D-Hpg) are fundamental side chain building blocks in many antimicrobial compounds, including the amoxicillin and vancomycin group of antibiotics.[1,2] Existing synthetic methods for the preparation of D-Phg and its derivatives rely on toxic cyanide chemistry and multi-step processes.[3] Alternative biocatalytic methods are limited by substrate solubility (*e.g.* the coupled hydantoinase/carbamoylase system), or rely on a D-amino acid aminotransferase that uses the costly D-amino acid donor and requires an additional enzyme (a racemase) to yield the desired product.[4,5] Aminotransferases (ATs, also known as transaminases, TAs or ATAs, EC 2.6.1)[6] are a large superfamily of pyridoxal 5′-phosphate (PLP)-dependent enzymes with a rapidly expanding range of industrial applications for the production of diverse compounds containing a chiral amine functionality.[7–15] For example, they have been shown to be a suitable replacement for a transition metal catalyst during the preparation of drugs such as sitagliptin.[16] ATs use PLP to catalyze the transfer of an amino group between an amino donor and an amino acceptor *via* a ping-pong, bi–bi mechanism *via* a pyridoxamine (PMP) form of the cofactor (Scheme 1).

The 3D structures of many PLP enzymes have been determined and they display seven different folds with TAs typically found in classes I and IV.[17–22] To determine the substrate scope of so many AT-catalysed reactions, powerful high-throughput assays have been developed that can be used to study the activities of wild-type ATs or identify new substrates for engineered enzymes.[23–27]

The X-ray structures and screening methods for these biocatalysts have been comprehensively reviewed[6] but there are many ATs that display "unusual" characteristics which require further study.

The D-phenylglycine aminotransferase (D-PhgAT), isolated from the soil bacterium *Pseudomonas stutzeri* ST-201[28,29]

[a] *School of Chemistry, University of Edinburgh, Joseph Black Building, David Brewster Road, Edinburgh, EH9 3FJ, UK. E-mail: Dominic.Campopiano@ed.ac.uk*
[b] *School of Natural and Environmental Sciences, Newcastle University, Newcastle upon Tyne, NE1 7RX, UK*
[c] *Institute for Molecular Plant Sciences, School of Biological Sciences, University of Edinburgh, King's Buildings, Edinburgh EH9 3BF, UK*

† The X-ray crystal structure of the D-PhgAT PLP-bound internal aldimine reported here is available in the Protein Data Bank (https://www.rcsb.org/) with the accession code 6G1F.

‡ Electronic supplementary information (ESI) available. See DOI: 10.1039/d0cy01391a

§ Current address: LEITAT Technological Center, Terrassa (Barcelona), Spain.
¶ Current address: Department of Chemistry, United Arab Emirates University, Al Ain (UAE).

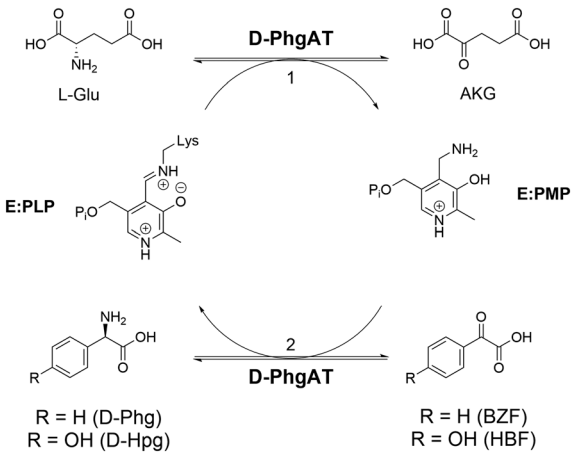

Scheme 1 Simplified, two-step mechanism of the D-PhgAT-catalysed reaction. In step 1, L-Glu donates the amino group to the pyridoxal 5′-phosphate (PLP) cofactor generating pyridoxal amine (PMP) and α-ketoglutarate (AKG). In step 2, benzoyl formate (BZF, R = H) or its 4′-hydroxy derivative (HBF, R = OH) accepts the amino group from PMP yielding D-Phg or D-Hpg respectively.[11]

catalyses the reversible transamination of L-glutamic acid (L-Glu) with the amino acceptors benzoylformate (BZF) and 4-hydroxy benzoylformate (HBF) yielding the *R*-enantiomers D-Phg and D-Hpg respectively. The keto product derived from L-Glu is α-ketoglutarate (AKG) (Scheme 1). What is unique to this AT is its so-called "stereo-inverting" characteristic, where the amino donors (L-Glu and D-Phg) in this reversible reaction exhibit inverse absolute configurations. Since it uses an inexpensive L- (or *S*-) amino acid donor, the *P. stutzeri* D-PhgAT represents an attractive biocatalyst for the synthesis of enantiomerically pure D-Phg (or *R*-Phg) derivatives in a single step.[5] D-PhgAT has also been used in qualitative and quantitative analysis of L-Glu concentrations in food when coupled with L-glutamate dehydrogenase[30] and for quality control of amoxicillin in pharmaceuticals when coupled with a penicillin acylase.[31] The homologous D-PhgAT from *P. putida*[32–34] (82% amino acid sequence identity) has been successfully combined with hydroxymandelate synthase (HmaS) and hydroxymandelate oxidase (Hmo) to engineer an *E. coli* strain that is able to produce D-Phg.[34]

To expand its potential as a valuable biocatalyst, comprehensive substrate and structural analyses of the *P. stutzeri* D-PhgAT are required. An understanding of the mechanism of its unique stereo-inverting activity will also aid in increasing its substrate scope by enzyme engineering.[35] In this study we describe the isolation of recombinant *P. stutzeri* D-PhgAT and, by a combination of spectrophotometric and chiral product analysis, we explore the amino substrate range and enantioselectivity of this enzyme. This revealed a broader substrate range than previously anticipated, which led us to use this biocatalyst to prepare a range of aromatic D-amino acids in high conversion and e.e. Furthermore, we determined the first X-ray structure of the PLP-bound form of the *P. stutzeri* D-PhgAT at 2.25 Å resolution, which confirms its classification as a member of the class III TA family. To explore the dual substrate binding mechanism, we then compared the D-PhgAT structure with the PLP-bound, external aldimine complexes of similar TAs. Furthermore, a combined sequence and structural analysis led to site-directed mutagenesis studies which identified potential residues required for catalytic activity and substrate recognition. This work lays the foundation for future enzyme engineering, and strengthens the utility of D-PhgAT as an important biocatalyst for the preparation of enantiopure D-aromatic amino acids.

Results and discussion

Recombinant, codon optimized, *P. stutzeri* D-PhgAT was produced in *E. coli* BL21 (DE3) with an N-terminal 6xHis affinity tag. It was purified to homogeneity in high yield by standard nickel affinity and gel-filtration chromatography methods, which showed it to be homodimeric in solution (Fig. S1‡). The enzyme shows a distinct UV/visible spectroscopic profile with a λ_{max} at 411 nm, indicative of PLP binding; this changes upon addition of the amino donor L-Glu and leads to PMP formation which absorbs at 311 nm (Fig. S2‡).

A convenient, high-throughput, coupled assay used the α-ketoglutarate dehydrogenase (AKGDH) enzyme to monitor transamination of L-Glu through NADH production (Fig. S3 and S4‡). This assay allowed the determination of kinetic parameters (apparent K_M for L-Glu and BZF are 9.85 ± 0.62 mM, 1.81 ± 0.57 mM respectively) in the "forward" D-amino acid-producing direction (Fig. S5, Table S1‡). We confirmed the chirality of the product using a modified Chirobiotic-T chiral HPLC method and demonstrated the enzyme enantioselectivity with production of D-Phg in >98% e.e. (Fig. S6 and S7‡).[36] Furthermore, we used this method to determine the D-PhgAT kinetics, which match well with the coupled assay (Fig. S8 and Table S1‡). With BZF as the amino acceptor the chiral HPLC assay was used to screen D-Phg production with various commonly used amino donors. These included L- and D-amino acids, *R*- and *S*-α-methylbenzylamine (MBA), isopropylamine (iPrA), as well as *o*-xylene diamine (OXD) (Fig. S9 and S10‡). The production of D-Phg is observed with several amino donors (apart from iPrA) and the activity is ranked relative to L-Glu as the best amino donor. This broad utility is in contrast with a previous report which observed a very limited substrate scope.[28] Regardless of the chirality of the amino donor, the enantiopurity of the final D-Phg product is not affected. Since L-Glu was the best amino donor it was used to scale up the reaction with 1 g BZF substrate. Using D-PhgAT (1 mg mL^{-1}) 93% conversion to D-Phg (99% e.e.) was observed after ~3 h (Fig. S11). We purified the D-Phg product by preparative HPLC (Fig. S12‡) and characterized it using ^1H and ^{13}C NMR and ESI-MS (Fig. S13‡) which are identical to an authentic standard.

Since D-Phe, D-Trp and D-Tyr are used as chiral building blocks for many clinically useful drugs, we tested the promiscuity of the *P. stutzeri* D-PhgAT towards various

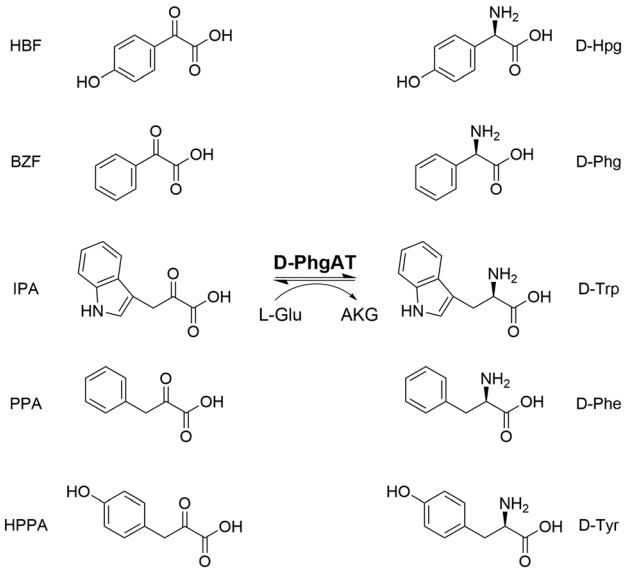

Scheme 2 D-PhgAT reactions for the synthesis of aromatic D-amino acids from L-Glu and aromatic amino acceptors.

aromatic acceptors.[37–39] We used D-PhgAT with L-Glu and the five amino acceptors (HBF, BZF, indole pyruvic acid (IPA), phenylpyruvic acid (PPA), and 4-hydroxyphenylpyruvic acid (HPPA)) that would yield the corresponding aromatic amino acids D-Hpg, D-Phg, D-Trp, D-Phe, and D-Tyr (Scheme 2). The enzyme shows good affinity towards all acceptor substrates tested (apparent K_M values from 0.79 mM for IPA to 9.24 mM for HPPA, Table 1).

Furthermore, we found again that the conversion was highly stereoselective with only the D-enantiomer produced (Fig. 1). Kinetic parameters and % conversions were calculated using the chiral HPLC method and are summarized in Table 1. Using this data larger scale biotransformations were carried out at up to 100 mg scale for each amino acceptor. The D-PhgAT displayed modest to excellent conversion for these aromatic acids, with the highest observed for the BZF to D-Phg conversion (93%). This analysis emphasizes the broad utility of the enzyme.

To understand the molecular basis of the substrate promiscuity and the origin of the D-enantioselectivity, as well as revealing the residues involved in catalysis, we determined the crystal structure of the D-PhgAT in complex with the PLP-cofactor bound as the internal aldimine form at 2.25 Å resolution (Fig. 2, S14 and S15‡). Here we used the incomplete structure of the *P. stutzeri* enzyme lacking the bound PLP cofactor (PDB code: 2CY8[40]) as a molecular replacement model (Table S2,‡ PDB code: 6G1F). The overall D-PhgAT structure confirmed its classification as a member of group III of the aspartate aminotransferase family, which falls within the type I PLP-dependent superfamily fold.[41]

The final refined model contains three homo-dimers of D-PhgAT with the PLP cofactor present as an internal aldimine bound to residue Lys269 in each chain (Fig. 2, S14 and S15‡). Each monomer can be subdivided into two

Table 1 Analysis of the D-PhgAT kinetic parameters with various amino acceptors. Kinetic parameters of D-PhgAT for five amino acceptors, obtained using the chiral HPLC method. Reactions were carried out for 15 minutes using 100 mM L-Glu and different amino acceptor concentrations (0–40 mM). To determine % conversions, reactions were carried out at 100 mg scale as described in the Experimental

Substrate	Conversion %	ee %	K_M (mM)	k_{cat}/K_M (M^{-1} s^{-1})
HBF	50	>98	1.01 ± 0.07	899.15 ± 0.27
BZF	93	>98	3.16 ± 0.46	302.80 ± 0.10
IPA	30	>98	0.39 ± 0.19	262.12 ± 0.13
PPA	57	>98	6.91 ± 0.99	14.49 ± 0.82
HPPA	15	>98	9.24 ± 2.40	0.06 ± 0.01

distinct domains: a small discontinuous domain comprising the residues 1–72 and 336–453; and a large domain formed by residues 73–335 (Fig. S14‡). The N-terminal part of the small domain comprizes a kinked α-helix followed by a three-stranded antiparallel β-sheet, while the C- terminal part consists of an α-helix followed by two antiparallel β-strands, an extended loop interspersed with a short α-helix and continues into a longer α-helix. This is followed by a β-strand that extends the N-terminal β-sheet and an additional β-strand, which extends the C-terminal β-sheet, the structure finishes with an α-helix opposed between the two other major helices in this domain. The large domain consists of a central seven-stranded β-sheet, with five parallel strands and two in an anti-parallel orientation. The β-sheet is connected by α-helices, which harbor the PLP cofactor binding site and main dimerization interface (Fig. S14‡).

The essential Lys269 is located in the loop that connects strands β9 and β10, with the aromatic ring of the PLP sandwiched between Val243 and Tyr149 (Fig. S15‡). Water molecules (red spheres) form bridges between the PLP phosphate oxygens and the side chains of Glu124, Thr303 and the backbone of Phe304 from the opposite monomer. The phosphate is also coordinated by H-bonds to Ser121, Gly122 and Thr123 from the same monomer.[42]

Since the ATs bind two amino-acid substrates, it has been proposed that this dual-substrate recognition is accommodated

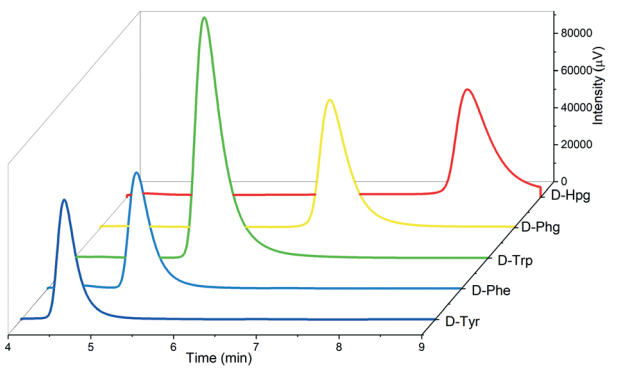

Fig. 1 Chiral HPLC traces of the synthesis of enantiopure D-Tyr, D-Phe, D-Trp, D-Phg and D-Hpg. Reactions described in Scheme 2 were analysed for product formation by chiral HPLC using a Chirobiotic T column with monitoring at λ = 205 nm.

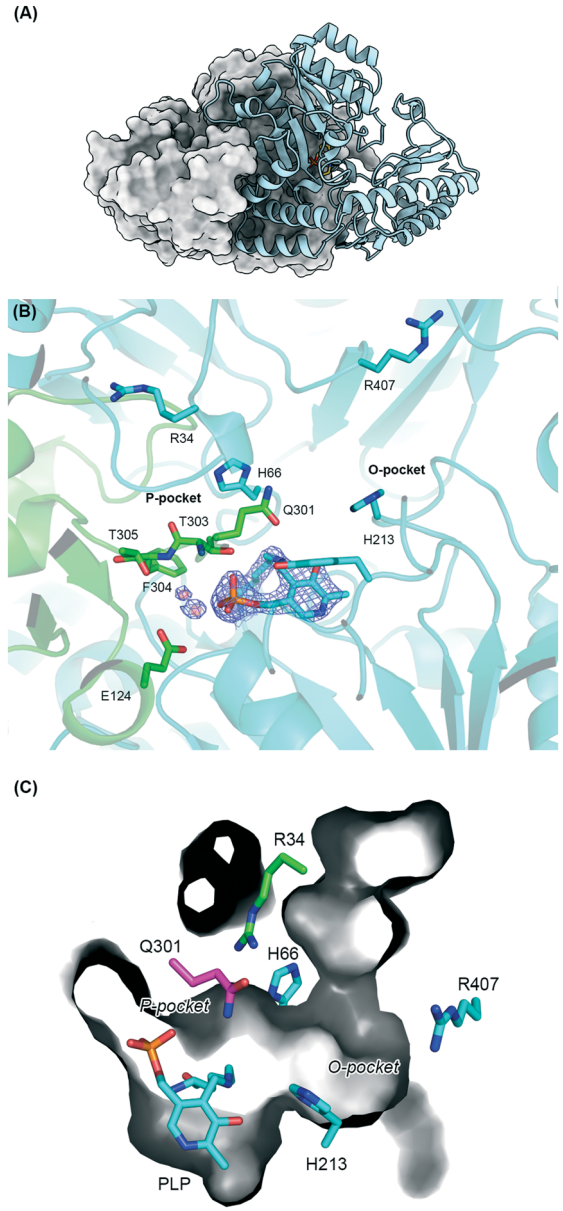

Fig. 2 Crystal structure of *P. stutzeri* D-PhgAT. (A) Functional dimer of the D-PhgAT protein, shown with one chain as a surface representation and the other as a cartoon showing the position of the PLP cofactor in stick representation. (B) Active site pockets of the D-PhgAT protein showing the PLP internal aldimine and key residues in the substrate binding pockets. The O- and P-pockets are labelled following the convention in Wybenga *et al.*[43] the protein backbone is shown as a cartoon, with key residues shown as sticks. The two chains in the structure are coloured green and blue. The final experimental 2mFo-DFc electron density for the PLP is shown as blue mesh. (C) Cut-away view of the substrate binding tunnel showing the depth and breadth of the active site region of the protein. Amino acids and PLP internal aldimine are shown as stick representations.

in two binding sites. These were named the O-pocket (or O-site, defined by the proximity of residues to the 3′-O of the PLP) and P-pockets (or P-site, defined by the proximity to the PLP-phosphate) by Dijkstra and colleagues in their study of the *S*-selective TA (*Mes*AT).[43] They determined the structures of this useful enzyme with the PLP-external aldimine forms of *S*-β-Phe and *R*-3-methylhexanoic acid, as well as with the amino acceptor AKG. These complexes allowed them to identify residues in the binding pockets as well as a pair of key arginine residues (Arg54 and Arg412) in this type I enzyme. The O- and P-pocket hypothesis was also explored by a comprehensive structural and sequence analysis of the AT superfamily recently carried out by Bornscheuer and colleagues to identify 13 key residues (including specific arginines) that they propose as crucial in controlling substrate binding and reaction specificity.[11] Bornscheuer and others have also put forward an elegant model known as the 'arginine flip or switch' that is thought to control the dual specificity of these enzymes.[44–47] By modelling into the incomplete apo D-PhgAT structure (2CY8) they suggested that a key Arg residue, equivalent to Arg407 in our structure, binds to the α-carboxylate of the L-Glu donor and may switch in and out of the active site. A recent paper by Walton *et al.* also determined the crystal structure of D-PhgAT (PDB code: 6DBS) and they used this to propose a two pocket substrate binding model and residues involved in catalysis.[48] Unfortunately, like 2CY8, the D-PhgAT had no PLP bound (but instead had phosphate) and lacked defined electron density for important residues 28–36 and 292–302.[42,48] These incomplete apo- and phosphate-bound structures are missing important features such as the P-pocket. In contrast, with the PLP bound in our structure we can now better define both pockets for the first time (Fig. 2B). The O-pocket is formed by the side chains of Phe63, His66, His213, Phe304, and Arg407. On the other side of the PLP cofactor the P-pocket is formed by residues Arg34, Gln301, and Thr303.

The enzyme is unusual in that it can bind both L- and D-forms of the amino acid substrates (*e.g.* L-Glu and D-Phg) depending on which reaction (forward or reverse) it is catalyzing (Schemes 1 and 2). This inherent substrate promiscuity of the enzyme and the product enantioselectivity appears to be due to a combination of these two pockets (Fig. 2B) and a cavity (Fig. 2C) that can accommodate large hydrophobic amino acceptors. This cavity extends from the surface of the protein and has a wide mouth with a constriction near the active site formed by the side chains of His66 and His213. This constriction accommodates hydrophobic substrates through pi-stacking interactions, while orienting the keto substrate to accept the amine group from the PMP intermediate. This results in the formation of the key PLP:substrate external aldimine intermediate that undergoes the enantiomeric H^+ transfer at C4′ to form the D-product (Fig. S16‡). We were also struck by the pair of arginine residues provided by one of the subunits, Arg34 (in the P-pocket) and Arg407 (in the O-pocket) (Fig. 2B). In the PLP bound structure, in the absence of an L-amino acid donor or a D-amino acid product, both of the side chains are orientated away from their respective pockets but are free to move upon ligand binding.

To understand how D-PhgAT bound its substrates Walton *et al.* superimposed the active sites of their PLP-free structure with MesAT with PLP and AKG (PDB: 2YKX), MesAT with

PLP:(*S*)-3-phenyl-β-alanine (PDB: 2YKY) and a GSAM AT with PLP:(4*S*)-4,5-diaminopentanoate (PDB: 2HP2).[48] The Arg54 and Arg412 side chains of MesAT were proposed to be equivalent residues to the Arg34 and Arg407 respectively in D-PhgAT. This allowed the "missing" Arg34 in the P-pocket to be proposed as the residue that engages the sidechain of the various substrates *e.g.* the γ-carboxylate of L-Glu. Similarly, in the O-pocket Arg407 is thought to interact with the carboxylate at the C-α of amino acids such as L-Glu.

Now with the Arg34-containing loop observed, we carried out similar structural comparisons of our PLP-bound structure with other TA enzymes to gain further insight into the residues involved in ligand binding in both pockets. We superimposed our PLP-bound internal aldimine structure with TAs that have structures with useful bound ligands. Here we used an interesting pair of *S*-selective ω-TAs, *Bacillus megaterium* (BM-ωTA) and *Arthrobacter* Ars-ωTA studied by Dijkstra and colleagues.[49] These enzymes share 95% sequence identity but surprisingly display somewhat different substrate profiles and structural studies revealed insights into their mechanism and specificity. The X-ray structure of the PLP:*R*-MBA external aldimine bound complex of the BM-ωTA (PDB code: 5G09,)[49] showed the phenyl group of *R*-MBA binding in the O-pocket and methyl group in the P-pocket.

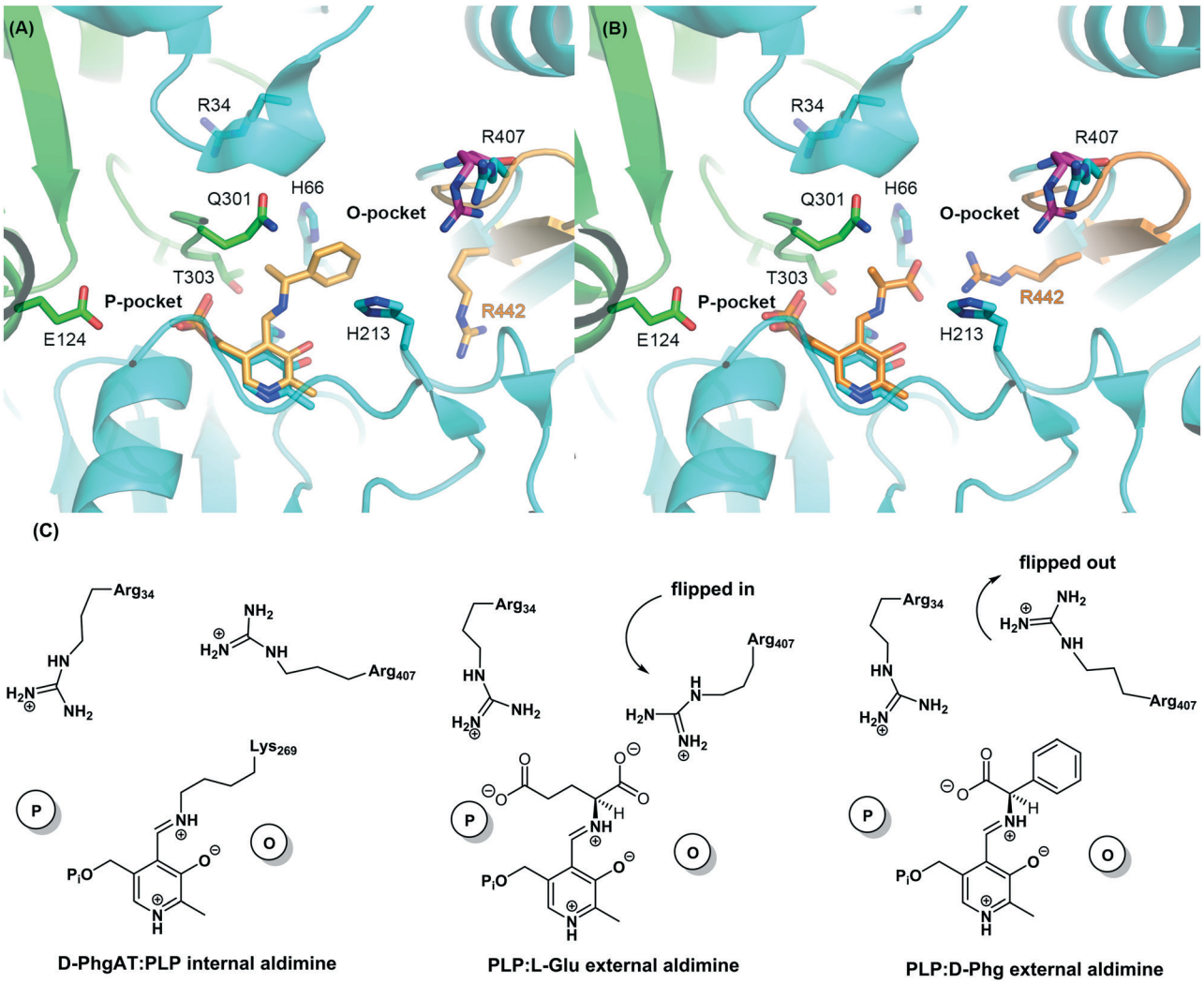

Fig. 3 Structural comparison of D-PhgAT with other aminotransferases. (A) Overlay of the *P. stutzeri* DPhgAT apo (6DVS, pink sticks) and PLP internal aldimine (6G1F, green and cyans cartoons and sticks) structures with the PLP:*R*-α-methylbenzylamine (*R*-α-MBA) external aldimine complex of the *B. megaterium S*-selective aminotransferase (5G09, orange). In the *B. megaterium* complex Arg442 swings away from the position of the ring of the *R*-α-MBA to accommodate this bulky intermediate. The equivalent residue in the *P. stutzeri* structure is Arg407, which is found in different conformations in the apo- and PLP-bound structures. (B) Overlay of the D-PhgAT:PLP internal aldimine with the PLP-external aldimine of Ars ω-TA PLP:L-Ala external aldimine complex (5G2Q). In Ars ω-TA PLP:L-Ala structure, the side chain of Arg442 swings in to interact with the C-α carboxylate of the PLP:L-Ala, this is a 180° flip around the CG of the arginine side chain in comparison to the *B. megaterium* structure. (C) Schematic representation of the dual substrate recognition mechanisms of D-PhgAT and the role of Arg34 and Arg407 in the arginine flip/switch model. In the forward direction the 'flipping' Arg407 in the O-pocket is involved in the recognition of the α-carboxylic group of amino donor L-Glu and can move out of the active site to accommodate the benzyl ring of the product D-Phg. In the P-pocket, the Arg34 side chain is involved in recognition of the α-carboxylate of the L-Glu (and L-Asp) amino donor.

Dijkstra and colleagues found that the O-pocket is large enough to accommodate the phenyl group, in contrast to the smaller P-pocket. The structure also revealed why this PLP:*R*-MBA external intermediate was captured in the unproductive state - the amine of the lysine 298 side chain is unable to act as a base since it is on the wrong face to remove the proton from C-α. By simply inverting the stereochemistry at C-α to the productive *S*-MBA configuration the enzyme could achieve the optimal orientation for catalysis. The D-PhgAT also prefers *S*-MBA to *R*-MBA (Fig. S9‡) suggesting a similar discrimination mechanism.

A comparison of the two structures (Fig. 3A) shows how this substrate could be accommodated into the O-pocket; in the BM-ωTA:PLP:*R*-MBA complex the Arg442 is swung out to make way for the phenyl ring and Arg407, the equivalent residue in D-PhgAT, is also swung out. Since D-PhgAT prefers L-Ala, L-Glu and L-Asp over their opposite enantiomers we also carried out a comparison (Fig. 3B) of the structure of the *Arthrobacter* Ars-ωTA in complex with the PLP:L-Ala external aldimine (5G2Q). In Ars-ωTA the side chain of Arg442 is proposed as the arginine switch; swung out in the PLP-bound complex and swung in to engage with the C-α carboxylate when L-Ala binds. Our overlay of suggests the D-PhgAT Arg407 residue plays the equivalent flipping role to Arg442 in Ars-ωTA. Our models also suggests that residues His66, His213 from one monomer and Thr303 from the partner monomer play a role in the enantioselective mechanism of the enzyme. These residues orientate the ligand to be protonated by Lys269 from the Si-face of the PLP-bound intermediate, generating the D-Phg enantiomer (Fig. 2B, S15 and S16‡).

We also used this structural analysis to rationalize the L- to D-stereoinversion selectivity of D-PhgAT. Proton transfer of the C-4′ of the resulting PLP:quinonoid intermediate is the key to the enantioselectivity and Jomrit *et al.*, determined that this occurred from the Si face of the intermediate.[50] The L-Glu and D-Phg must bind in inverted orientations with respect to each other. The aromatic side chain of D-Phg (and the other aromatic amino acids we generated) must therefore exchange for the C-α carboxylate of L-Glu (O-pocket) and, similarly, the carboxylate at C-α of D-Phg can swap into the site (P-pocket) that binds the γ-carboxylate of the L-Glu side chain. This conformational flexibility requires mobile side chains in the two pockets and the two arginine residues (R34 and R407) have the ability to provide such dynamic movement. They are ideally placed to be able to swing in to engage with carboxylate residues directly in electrostatic interactions. Clearly, the active site must be highly dynamic during catalytic cycles that bind and release amino acceptors and products, depending on which direction it is operating (Schemes 1 and 2). Moreover, we also noted the presence of Q301 in the P-pocket in our structure, and this adds further weight to its important role in the catalytic mechanism. The importance of Q301 was identified in a recent cell-free extract, high-throughput, saturation mutagenesis screen of D-PhgAT catalysing the reverse reaction of D-Phg conversion to L-Glu.[48] This contrasts with our assay which monitors aromatic amino acid production and AKG release. In their screen Walton *et al.* focused on three residues in the O-pocket (H66, H213 and R407) and two, in what they predicted, in the absence of defined electron density, to be the P-pocket (R34 and Q301). It is interesting to note that, like us, they also found D-PhgAT displayed some substrate promiscuity – D-Phg was the best substrate but also showed ~8.6% relatively activity with D-Trp and ~82% relative activity with (*S*-)-4-phenyl-4-aminobutyrate.

We gained further insight into the properties of D-PhgAT by carrying out a sequence alignment of the two D-PhgATs from *P. stutzeri* and *P. putida* with well characterized ATs from the same group III fold, but with opposite product enantioselectivity (Fig. S17‡). This revealed that the key residues (Arg34, His66, His213, Gln301 and Arg407) identified in our structural analysis are found only in the stereo-inverting enzymes (also referred to as *R*-selective) that produce D-products from L-amino acid donors. This suggests that this stereo-inverting property has arisen from using the group III TA fold and incorporating these four key amino acids. Since we found these arginine residues in the active site, we carried out a targeted mutagenesis study and mutants of these two residues, R34A and R407A, as well as the two histidine residues, H66A and H213A, were obtained. We also included the Q301A mutant to allow comparison with the recent results presented by Walton *et al.*[48] The results of this mutagenesis study, summarized in Table 2, show the effect of these changes on the affinity and catalytic efficiency towards both L-Glu and BZF in the forward, D-Phg synthesis direction.

As we predicted, the two arginine mutants R34A and R407A displayed a much lower affinity towards L-Glu with a K_M of 368.33 (~14 fold) and 133.50 mM (~5 fold) respectively *vs.* the wild-type K_M of 26.17 mM. The k_{cat} and the catalytic efficiency is substantially disrupted by the mutations for both substrates by approximately 200- and 20-fold respectively. The proposed role of Arg34 as a key residue in binding L-Glu is strengthened since we found it was not possible to saturate the enzyme with the highest achievable concentration of L-Glu in the assay (500 mM). Like all AT enzymes, the catalytic cycle involves many PLP-derived intermediates including the true amine donor PMP which delivers the $-NH_2$ group to AKG to give D-Phg in that direction. In the absence of PLP-bound intermediate structures we used our combined sequence, structural and mutagenesis results to envisage how the substrates and products are recognized (Fig. 3C). We suggest that Arg407 is the key "flipping" residue that recognizes the C-α carboxylate of the L-Glu amino donor as well as being able to make way for the side chains of the aromatic products. Its partner Arg34 is involved in the recognition of the amino donor side chain carboxylic acid group, L-Glu is preferred but the shorter L-Asp can also be accepted. This arginine 'switch' and substrate promiscuity requires a flexible side chain and the mobility of Arg407 was revealed by comparing our PLP-bound structure with the two apo-D-PhgAT structures (PDBID:2CY8 and PDBID:6DVS).[40,50] We found that this sidechain adopts a different orientation

Table 2 Kinetic analysis of the D-PhgAT mutants. Summary of the kinetic parameters of D-PhgAT WT and mutants for the BZF and L-Glu substrates

	L-Glu			BZF		
D-PhgAT	K_M (mM)	k_{cat} (s^{-1})	k_{cat}/K_M (M^{-1} s^{-1})	K_M (mM)	k_{cat} (s^{-1})	k_{cat}/K_M (M^{-1} s^{-1})
WT	26.17 ± 3.63	1.65 ± 0.12	63.21 ± 0.78	3.16 ± 0.46	0.95 ± 0.056	302.80 ± 0.10
R34A[a]	368.33 ± 18.78	0.111 ± 0.0088	0.304 ± 0.004	0.842 ± 0.15	0.079 ± 0.016	93.33 ± 0.037
R407A	133.50 ± 30.5	0.42 ± 0.012	3.22 ± 0.09	1.51 ± 0.45	0.169 ± 0.012	112.98 ± 0.12
H66A	9.65 ± 0.32	0.092 ± 0.006	9.76 ± 0.009	11.66 ± 5.95	0.078 ± 0.01	9.57 ± 0.09
H213A	—	—	—	—	—	—
Q301A	43.23 ± 7.90	0.38 ± 0.015	20.59 ± 0.020	9.02 ± 0.95	0.15 ± 0.012	16.43 ± 0.05

[a] The K_M could not be accurately determined as the highest achievable amount of L-Glu in the reaction was 500 mM.

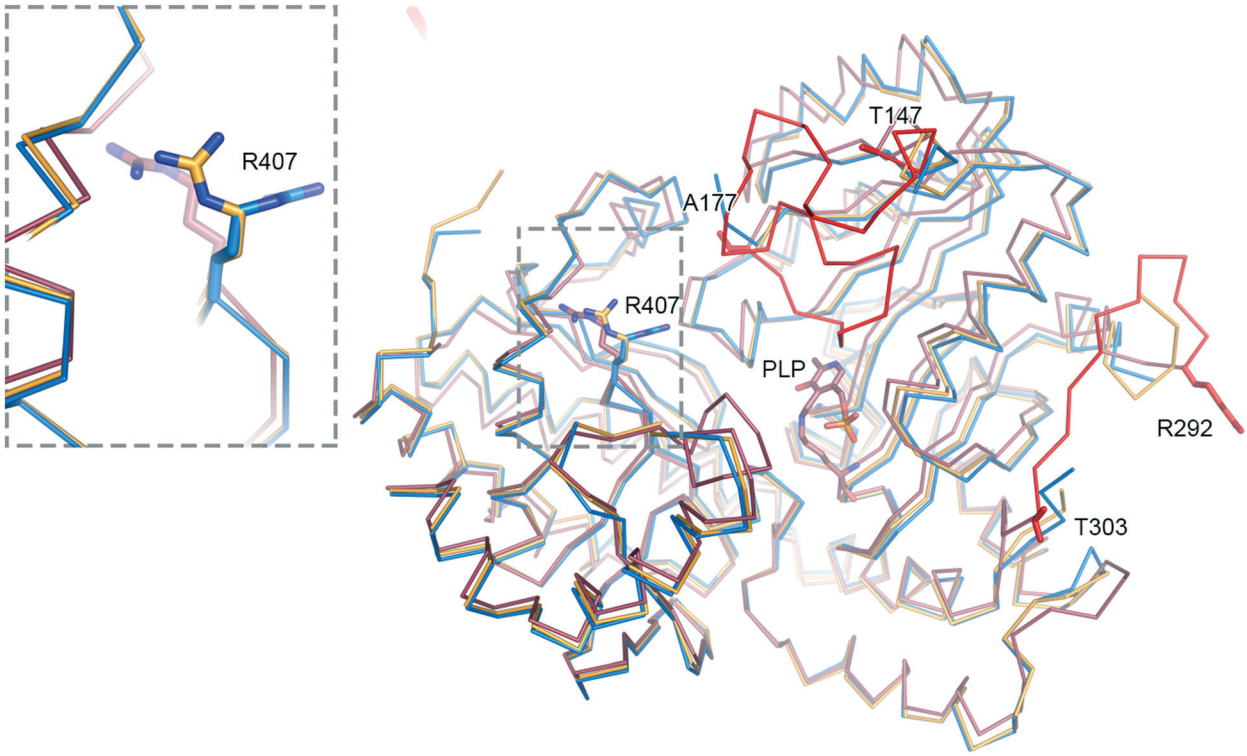

Fig. 4 Comparison of apo- and PLP-bound forms of D-PhgAT highlights the mobility and movement of Arg407 and loops around PLP-binding site. Our PLP-bound structure shown in salmon with two apo-forms in orange (PDBID: 2CY8) and blue (PDBID: 6DVS). The disordered, flexible loops, defined only in the PLP-bound structure, are shown as red ribbons with terminal ordered residues labelled and shown as sticks. For clarity the inset shows a zoom in of the positions of the Arg407 residue in each structure.

in each structure, suggesting that it is able to move to accommodate substrate binding during catalysis (Fig. 4).

The H213A mutant was totally inactive in all the tested conditions, suggesting that this residue is crucial to positioning the substrate in the O-pocket. This is in contrast to the H213A mutant described by Walton *et al.* which displays ~45% activity in the reverse direction. Interestingly, H213N was 150% more active than the wild type but a rationale for this dramatic increase is not clear. In our hands both the H66A and Q301A mutants retained some activity and by analysis of the structure we suggest that these residues are involved in amino-acceptor binding and a hydrogen bonding network surrounding the PLP cofactor respectively (Fig. S15‡). Similarly, in their screen Walton *et al.* found that mutations at H66 and Q301 resulted in diminished activity.

Conclusions

In conclusion, using the *P. stutzeri* D-PhgAT we describe a biocatalytic approach to a preparative-scale synthesis of D-Phg in high % e.e. and yield. The widespread use of PLP-dependent ATs for industrial biotechnology has been hampered by the unfavorable reaction equilibrium towards product formation. This can be overcome by the use of "smart amine donors", coupled recycling systems or removal of the keto co-product.[24,51,52] Unfortunately, the commonly used iPrA was not accepted by D-PhgAT so here we used a large excess of the inexpensive amino donor L-Glu (~20 times K_M) to drive the equilibrium towards product formation. Our optimized system gives conversions (93%) that are higher than those previously reported.[28]

A recent report described the engineering of three recombinant *E. coli* strains that co-expressed four, seven and nine enzymes, including the *P. stutzeri* D-PhgAT as the final step. These whole cell biotransformations produced a range of D-Phg derivatives in one pot from racemic mandelic acid, styrene and L-Phe starting materials.[53] Since we have shown the D-PhgAT to be a versatile biocatalyst in being able to use a range of amino acceptors it suggests that similar cascades could be constructed to allow conversion of simple building blocks to produce a variety of enantiopure aromatic D-amino acids.[53]

The determination of the first crystal structure of the D-PhgAT with its bound PLP cofactor has shed light on the unique stereo-inverting and enantioselective properties of the enzyme. The broad substrate scope is explained by a large active site cavity and two pockets each containing an essential Arg residue that is crucial for the catalytic activity. Our study highlights key active site residues that are involved in the catalytic mechanism and potentially control the exquisite *R*-selectivity of the enzyme. These features suggest that the O-pocket of D-PhgAT could be engineered to accept even bulkier pro-chiral substrates and convert them to enantiopure *R*-products. Our study paves the way for D-PhgAT engineering in order to further expand the substrate scope of this enzyme.[54,55] In future, structures of the enzyme with substrates and products, combined with a directed evolution campaign, will allow the product scope of D-PhgAT to be further expanded to take advantage of the unique properties of this versatile biocatalyst.

Experimental

General

Standard chemical reagents (D-Phg, D-Hpg, or other amino acids, CoASH, buffers) and enzymes were from Sigma, VWR, Alfa Aesar and Acros Organic.

Cloning and protein expression

The full-length, codon optimized dpgA gene (*Pseudomonas stutzeri* ST-201, UNIPROT code: Q6VY99) was purchased from GenScript and cloned into pET 15b plasmid to give a recombinant D-PhgAT with a non-cleavable N-terminal His6-tag. The construct was used to transform *E. coli* BL21 (DE3) competent cells and selection was carried out on agar plates containing ampicillin (100 μg mL^{-1}; LB/Amp_{100}). A single colony was used to inoculate 250 mL of LB/Amp_{100} broth and the overnight culture was grown at 37 °C with shaking at 250 rpm. The overnight culture was used to inoculate 1 L of fresh LB/Amp_{100} broth and grown to an A_{600} of 0.6–0.9. Protein expression was induced by addition of IPTG to a final concentration of 0.1 mM and growth was continued for 16 h at 20 °C. Cells were harvested by centrifugation (Thermo Scientific Multicentrifuge X3R) at 4000 × *g* for 30 min at 4 °C.

Site directed mutagenesis

The D-PhgAT R34A, H66A, H213A, Q301A and R407A mutants were constructed according to the overlapping primer site-directed mutagenesis (SDM) method with the primer pairs outlined in the supporting information. Colonies were picked and sequenced, and based on the results, mutants were taken forward for analysis. The mass of each D-PhgAT mutant was confirmed by LC electrospray ionization mass spectrometry (ESI-MS).

D-PhgAT purification

All purification steps were carried out at 4 °C. Cells were resuspended in lysis buffer (0.1 M CAPS pH 9.5, 150 mM NaCl, 20 mM imidazole, 50 μM PLP) with the addition of DNase (0.2 mg per 10 mL buffer) and lysed by sonication for 15 cycles (30 s on, 30 s off). The lysed cell suspension was cleared by centrifugation (Thermo Scientific Multicentrifuge X3R) at 14 000 × *g* for 40 min at 4 °C. The cell-free extract was loaded onto a 1 mL HisTrap nickel affinity column (GE Healthcare). The column was washed with binding buffer for 20 column volumes, then the protein eluted with an imidazole gradient (10 to 500 mM) over 30 column volumes. Protein containing fractions were analysed by 12% SDS-PAGE and concentrated to 1 mL using the Vivaspin 20 MWCO 30000 (Sartorius). The concentrated D-PhgAT was loaded onto a pre-equilibrated (0.1 M CAPS, 150 mM NaCl, 50 μM PLP) HiPrep™ 16/600 Superdex™ S-200 size exclusion column (120 mL). Recombinant protein was eluted at a flow rate of 1 mL min^{-1} in buffer. The purity of the recombinant proteins was analysed by 12% SDS-PAGE.

Spectroscopic analysis

All UV-visible spectra were recorded on a single-beam Cary 50 UV-vis spectrometer and analysed using Origin. To convert the apo-D-PhgAT to the holo-D-PhgAT form the enzyme was dialyzed for 2 h at 4 °C against 0.1 M CAPS (pH 9.5) containing 150 μM NaCl and 50 μM PLP. Excess PLP was removed by passing the protein through a PD-10 (Sephadex G- 25M) de-salting column (GE Healthcare) before any spectrophotometric measurements were taken. The concentration of recombinant D-PhgAT was 20 μM and the spectrophotometer was blanked with 0.1 M CAPS (pH 9.5) containing 150 mM NaCl and 50 μM PLP.

α-Ketoglutarate dehydrogenase assay (AKGDH assay)

The D-PhgAT activity was monitored by coupling the reaction with the α-ketoglutarate dehydrogenase (AKGDH) since α-ketoglutarate (AKG) is the product of the first half reaction. The final volume of the reactions was 250 μl and contained 0.1 M CAPS pH 9.5, 150 mM NaCl, 1 mM $MgCl_2$, 1 mM $CaCl_2$, 0.05 mM EDTA, 50 μM PLP, 1 mM CoASH, 3 mM NAD^+, 0.2 U KGDH, 0 to 50 mM L-Glu, 0 to 20 mM benzylformate (BZF). These reagents were pre-incubated at 35 °C and the reaction was blanked. The reaction was initiated by adding 1 μM D-PhgAT. The increase in absorbance at 340 nm resulting from the enzymatic conversion of NAD^+ to NADH after AKG production by the D-PhgAT was monitored over 1 h on a BioTek Synergy HT

plate reader with Costar 96-well plate. The data from the first 15 min were analyzed using the Michaelis–Menten model and a nonlinear regression fit on GraphPad gave values of K_M and k_{cat} (ε_{NADH} = 6220 M^{-1} cm^{-1}).

High performance liquid chromatography (HPLC) analysis

For the HPLC method, reactions containing 0.51 mg mL^{-1} D-PhgAT, 0–200 mM L-Glu, 0–20 mM amino acceptors (BZF/HBZF/IPA/PPA/HPA) in 0.1 M CAPS pH 9.5, 150 mM NaCl, 50 μM PLP buffer were incubated at 37 °C before being terminated at 15 minutes by diluting 40 fold in the chiral mobile phase: 0.025% triethylammonium acetate (TEAA) : MeOH (50 : 50). Reactions were then analysed by chiral HPLC using a Chirobiotic T column (Astec, chiral phase Teicoplanin, 5 μm, 250 mm × 4.6 mm) and the following isocratic conditions: mobile phase: 0.025% TEAA : MeOH (50 : 50, v/v), flow rate: 1 mL min^{-1}, λ: 205 nm, temperature: RT, run time: 30 min. The column was calibrated with single enantiomers of the amino acids. The conversion was used to measure enzyme activity. For the detection of non-natural substrates such as D-phenylalanine, D-tyrosine and D-tryptophan the same procedure was applied. Lab solution software (Shimadzu) was used to measure the area under the product peaks. To determine the kinetic parameters, reactions were carried out in triplicate and quenched after 15 minutes by 1 : 40 dilution in the chiral mobile phase. The data were analyzed using the Michaelis–Menten model and a nonlinear regression fit on GraphPad The data points were taken as the average values, with the errors calculated as the standard deviations.

Amino donor screening

A D-PhgAT aliquot was thawed and incubated on ice with 50 μM PLP for ~2 h in order to be sure it was fully loaded with fresh PLP.

Reactions containing 0.51 mg mL^{-1} D-PhgAT, 10 mM L/D amino donor, 10 mM BZF in 0.1 M CAPS pH 9.5, 150 mM NaCl, 50 μM PLP buffer were incubated at 37 °C before being terminated at 18 h by diluting 40-fold in the chiral mobile phase. Reactions were then analysed by chiral HPLC using a Chirobiotic-T column as stated before. Percentage conversions were normalized relative to L-Glu as the best amino donor.

Biotransformation reactions

The large scale biotransformation was performed in a 100 mL conical flask in a final volume of 20 mL. For each component of the reaction the pH was adjusted to 9.5 before being added to the reaction mixture. Freshly purified D-PhgAT (loaded with PLP) was added at a final concentration of 0.2 mg mL^{-1}, 0.4 mg mL^{-1} or 1 mg mL^{-1} (4 μM, 8 μM, 20 μM) in 0.1 M CAPS buffer pH 9.5, 150 mM NaCl, 50 μM PLP containing 1 g of BZF (~133 mM) and 500 mM L-Glu. The biotransformation was carried out at 37 °C at 120 rpm. A negative control with all the reagents omitting the enzyme was performed at the same time. Time points were collected at time 0, 15 min, 30 min, 1 h, 2 h, 3 h, 4 h, 5 h, 6 h, 7 h, 8 h, 9 h, 24 h, 36 h. Each time point was collected in triplicated and processed as described above. At each time point reactions were terminated by diluting 40 fold in the chiral mobile phase and analysed by HPLC.

X-ray crystallography

Purified D-PhgAT, at 9.1 mg mL^{-1}, was crystallized by hanging-drop vapor diffusion at 18 °C. Yellow crystals were produced by adding 1 μL of 9.1 mg mL^{-1} D-PhgAT in 0.1 M CAPS (pH 9.5), 150 mM NaCl, 50 μM PLP to 1 μL of 0.1 M TrisHCl (pH 7.5), 0.2 M $MgCl_2$, 10% (v/v) polyethylene glycol 8000 (PEG 8000). Crystals were cryo-protected with a solution containing 0.1 M TrisHCl (pH 7.5), 0.2 M $MgCl_2$, 10% (v/v) polypropylene glycol 8000, 20% (v/v) polypropylene glycol 200 PEG and then flash-cooled by immersion in liquid nitrogen. Datasets were collected on beamline I03 at the Diamond Light Source (Didcot, UK) at 100 K using a Pilatus 6 M detector. Diffraction data were integrated and scaled using XDS 46 and symmetry-related reflections were merged with Aimless. The resolution cut off used for structure determination and refinement was determined based on the CC1/2 criterion proposed by Karplus and Diederichs. The structure of D-PhgAT was determined by molecular replacement using the D-PhgAT incomplete structure with the PDB code 2CY8. A single solution comprising three dimers in the asymmetric unit was found using Phaser. The initial model was rebuilt using Phe-nix.autobuild followed by cycles of refinement with Phenix.refine and manual rebuilding in Coot. The final model was refined with automatically determined TLS groups and isotropic B-factors. The model was validated using MolProbity. Structural superimpositions were calculated using Coot. Crystallographic figures were generated with PyMOL (Schrodinger LLC). Data collection and refinement statistics are shown in Table S2.‡ X-ray diffraction images are available online at Zendo (doi:10.5281/zenodo.1059413).

Crystal structures were overlayed using the Pymol Align feature within Pymol (The PyMOL Molecular Graphics System, Version 1.2r3pre, Schrödinger, LLC). The RMSD values for each overlay are: 6G1F with 5G2Q – 2.18 Å over 1610 atoms; 6G1F with 5G09 – 2.12 Å over 1546 atoms; 6G1F with 6DVS – 0.351 Å over 2205 Å.

Conflicts of interest

The authors report no conflicts of interest with this work.

Acknowledgements

We thank the Industrial Biotechnology Innovation Centre (IBIOIC) for a PhD studentship (AS) and proof of concept funding (MKA). We thank the EPSRC CRITICAT Centre for Doctoral Training for the award of a PhD studentship (to SDC, EP/L016419/1).

Notes and references

1 B. K. Hubbard, M. G. Thomas and C. T. Walsh, *Chem. Biol.*, 2000, **7**, 931–942.
2 R. S. Al Toma, C. Brieke, M. J. Cryle and R. D. Süssmuth, *Nat. Prod. Rep.*, 2015, **32**, 1207–1235.
3 M. A. Wegman, M. H. A. Janssen, F. van Rantwijk and R. A. Sheldon, *Adv. Synth. Catal.*, 2001, **343**, 559–576.
4 W. Leuchtenberger, K. Huthmacher and K. Drauz, *Appl. Microbiol. Biotechnol.*, 2005, **69**, 1–8.
5 J. M. Choi, S. S. Han and H. S. Kim, *Biotechnol. Adv.*, 2015, **33**, 1443–1454.
6 I. Slabu, J. L. Galman, R. C. Lloyd and N. J. Turner, *ACS Catal.*, 2017, **7**, 8263–8284.
7 A. Gomm and E. O'Reilly, *Curr. Opin. Chem. Biol.*, 2018, **43**, 106–112.
8 S. A. Kelly, S. Pohle, S. Wharry, S. Mix, C. C. R. Allen, T. S. Moody and B. F. Gilmore, *Chem. Rev.*, 2018, **118**, 349–367.
9 F. Guo and P. Berglund, *Green Chem.*, 2017, **19**, 333–360.
10 F. Steffen-Munsberg, C. Vickers, H. Kohls, H. Land, H. Mallin, A. Nobili, L. Skalden, T. van den Bergh, H.-J. Joosten, P. Berglund, M. Höhne and U. T. Bornscheuer, *Biotechnol. Adv.*, 2015, **33**, 566–604.
11 S. Chen, H. Land, P. Berglund and M. S. Humble, *J. Mol. Catal.*, 2016, **124**, 20–28.
12 M. Fuchs, J. E. Farnberger and W. Kroutil, *Eur. J. Org. Chem.*, 2015, **2015**, 6965–6982.
13 W. Kroutil, E.-M. Fischereder, C. S. Fuchs, H. Lechner, F. G. Mutti, D. Pressnitz, A. Rajagopalan, J. H. Sattler, R. C. Simon and E. Siirola, *Org. Process Res. Dev.*, 2013, **17**, 751–759.
14 P. P. Taylor, D. P. Pantaleone, R. F. Senkpeil and I. G. Fotheringham, *Trends Biotechnol.*, 1998, **16**, 412–418.
15 N. J. Turner and E. O'Reilly, *Nat. Chem. Biol.*, 2013, **9**, 285–288.
16 C. K. Saville, J. M. Janey, W. R. Jarvis, J. C. Colbeck, A. Krebber, F. J. Fleitz and J. Brands, *Science*, 2010, **329**, 305–310.
17 G. Schneider, H. Käck and Y. Lindqvist, *Structure*, 2000, **8**, R1–R6.
18 F. W. Alexander, E. Sandmeier, P. K. Mehta and P. Christen, *Eur. J. Biochem.*, 1994, **219**, 953–960.
19 K. Hirotsu, M. Goto, A. Okamoto and I. Miyahara, *Chem. Rec.*, 2005, **5**, 160–172.
20 A. Paiardini, R. Contestabile, A. M. Buckle and B. Cellini, *BioMed Res. Int.*, 2014, **2014**, 856076.
21 M. L. Salvo, N. Budisa and R. Contestabile, *Chem. Rev.*, 2012, **118**, 27–66.
22 R. A. John, *Biochim. Biophys. Acta*, 1995, **1248**, 81–96.
23 S. Schätzle, M. Höhne, E. Redestad, K. Robins and U. T. Bornscheuer, *Anal. Chem.*, 2009, **81**, 8244–8248.
24 D. Baud, N. Ladkau, T. S. Moody, J. M. Ward and H. C. Hailes, *Chem. Commun.*, 2015, **51**, 17225–17228.
25 M. D. Truppo, J. D. Rozzell, J. C. Moore and N. J. Turner, *Org. Biomol. Chem.*, 2009, **7**, 395–398.
26 E. Heuson, J.-L. Petit, A. Debard, A. Job, F. Charmantray, V. de Berardinis and T. Gefflaut, *Appl. Microbiol. Biotechnol.*, 2016, **100**, 397–408.
27 J. Hopwood, M. D. Truppo, N. J. Turner and R. C. Lloyd, *Chem. Commun.*, 2011, **47**, 773–775.
28 S. Wiyakrutta and V. Meevootisom, *J. Biotechnol.*, 1997, **55**, 193–203.
29 K. Jariyachawalid, P. Laowanapiban, V. Meevootisom and S. Wiyakrutta, *Microb. Cell Fact.*, 2012, **11**, 47.
30 W. Khampha, V. Meevootisom and S. Wiyakrutta, *Anal. Chim. Acta*, 2004, **520**, 133–139.
31 T. Rojanarata, P. Opanasopit, T. Ngawhirunpat, C. Saehuan, S. Wiyakrutta and V. Meevootisom, *Enzyme Microb. Technol.*, 2010, **46**, 292–296.
32 W. J. J. van den Tweel, J. P. Smits and J. A. M. de Bont, *Arch. Microbiol.*, 1986, **144**, 169–174.
33 W. J. J. van den Tweel, J. P. Smits, R. L. H. P. Ogg and J. A. M. de Bont, *Appl. Microbiol. Biotechnol.*, 1988, **29**, 224–230.
34 U. Müller, F. van Assema, M. Gunsior, S. Orf, S. Kremer, D. Schipper, A. Wagemans, C. A. Townsend, T. Sonke, R. Bovenberg and M. Wubbolts, *Metab. Eng.*, 2006, **8**, 196–208.
35 U. T. Bornscheuer, G. W. Huisman, R. J. Kazlauskas, S. Lutz, J. C. Moore and K. Robins, *Nature*, 2012, **485**, 185–194.
36 S. Baxter, S. Royer, G. Grogan, F. Brown, K. E. Holt-Tiffin, I. N. Taylor, I. G. Fotheringham and D. J. Campopiano, *J. Am. Chem. Soc.*, 2012, **134**, 19310–19313.
37 N. Tentolouris, C. Voulgari and N. Katsilambros, *Vasc. Health Risk Manage.*, 2007, **3**, 797–807.
38 I. Kepert, J. Fonseca, C. Müller, K. Milger, K. Hochwind, M. Kostric, M. Fedoseeva, C. Ohnmacht, S. Dehmel, P. Nathan, S. Bartel, O. Eickelberg, M. Schloter, A. Hartmann, P. Schmitt-Kopplin and S. Krauss-Etschmann, *J. Allergy Clin. Immunol.*, 2017, **139**, 1525–1535.
39 K. A. Hansford, R. C. Reid, C. I. Clark, J. D. A. Tyndall, M. W. Whitehouse, T. Guthrie, R. P. McGeary, K. Schafer, J. L. Martin and D. P. Fairlie, *ChemBioChem*, 2003, **4**, 181–185.
40 P. Kongsaeree, C. Samanchart, P. Laowanapiban, S. Wiyakrutta and V. Meevootisom, *Acta Crystallogr., Sect. D: Biol. Crystallogr.*, 2003, **59**, 953–954.
41 J. Catazaro, A. Caprez, A. Guru, D. Swanson and R. Powers, *Proteins*, 2014, **82**, 2597–2608.
42 A. I. Denesyuk, K. A. Denessiouk, T. Korpela and M. S. Johnson, *J. Mol. Biol.*, 2002, **316**, 155–172.
43 G. G. Wybenga, C. G. Crismaru, D. B. Janssen and B. W. Dijkstra, *J. Biol. Chem.*, 2012, **287**, 28495–28502.
44 A. Eliot and J. Kirsch, *Annu. Rev. Biochem.*, 2004, **73**, 383–415.
45 V. N. Malashkevich, J. J. Onuffer, J. F. Kirsch and J. N. Jansonius, *Nat. Struct. Biol.*, 1995, **2**, 548–553.
46 S. Kamitori, A. Okamoto, K. Hirotsu, T. Higuchi, S. Kuramitsu, H. Kagamiyama, Y. Matsuura and Y. Katsube, *J. Biochem.*, 1990, **108**, 175–184.
47 F. Steffen-munsberg, C. Vickers, A. Thontowi, S. Schätzle, T. Meinhardt, S. Humble, H. Land, P. Berglund, U. T. Bornscheuer and M. Hçhne, *ChemCatChem*, 2013, **5**, 154–157.
48 C. J. W. Walton, F. Thiebaut, J. S. Brunzelle, J.-F. Couture and R. A. Chica, *Biochemistry*, 2018, **57**, 5437–5446.

49 N. van Oosterwijk, S. Willies, J. Hekelaar, A. C. Terwisscha van Scheltinga, N. J. Turner and B. W. Dijkstra, *Biochemistry*, 2016, **55**, 4422–4431.
50 J. Jomrit, P. Summpunn, V. Meevootisom and S. Wiyakrutta, *Biochem. Biophys. Res. Commun.*, 2011, **405**, 626–631.
51 A. P. Green, N. J. Turner and E. O'Reilly, *Angew. Chem., Int. Ed.*, 2014, **53**, 10714–10717.
52 A. Gomm, W. Lewis, A. P. Green and E. O'Reilly, *Chemistry*, 2016, **22**, 12692–12695.
53 Y. Zhou, S. Wu and Z. Li, *Adv. Synth. Catal.*, 2017, **359**, 4259.
54 F. H. Arnold, *Angew. Chem., Int. Ed.*, 2018, **57**, 4143–4148.
55 N. J. Turner, *Nat. Chem. Biol.*, 2009, **5**, 567–573.